

# Spatial distributions of magnetic field in the RHIC and LHC energy regions<sup>\*</sup>

ZHONG Yang(钟洋)<sup>1,2;1)</sup> YANG Chun-Bin(杨纯斌)<sup>1,3</sup> CAI Xu(蔡勖)<sup>1,3</sup> FENG Sheng-Qin(冯笙琴)<sup>2,3</sup>

<sup>1</sup> Institute of Particle Physics, Central China Normal University, Wuhan 430079, China

<sup>2</sup> College of Science, China Three Gorges University, Yichang 443002, China

<sup>3</sup> Key Laboratory of Quark and Lepton Physics (MOE), Central China Normal University, Wuhan 430079, China

**Abstract:** Relativistic heavy-ion collisions can produce extremely strong magnetic fields in the collision regions. The spatial variation features of the magnetic fields are analyzed in detail for non-central Pb–Pb collisions at LHC at  $\sqrt{s_{NN}}=900, 2760$  and  $7000$  GeV and Au–Au collisions at RHIC at  $\sqrt{s_{NN}}=62.4, 130$  and  $200$  GeV. The dependencies of magnetic field on proper time, collision energies and impact parameters are investigated in this paper. It is shown that an enormous and highly inhomogeneous spatial distribution magnetic field can indeed be created in off-centre relativistic heavy-ion collisions in RHIC and LHC energy regions. The enormous magnetic field is produced just after the collision, and the magnitude of magnetic field of the LHC energy region is larger than that of the RHIC energy region at small proper time. It is found that the magnetic field in the LHC energy region decreases more quickly with the increase of proper time than that of the RHIC energy region.

**Key words:** the distribution of magnetic field, non-central collision

**PACS:** 25.75.Ld, 11.30.Er, 11.30.Rd      **DOI:** 10.1088/1674-1137/39/10/104105

## 1 Introduction

Many analytical and numerical calculations indicate the existence of extremely powerful electromagnetic fields in non-central collisions of relativistic heavy-ion collisions [1–4]. These are the strongest electromagnetic fields that exist in nature. Refs. [5, 6] discuss the electromagnetic response of the plasma produced by relativistic heavy-ion collisions. It is found that these effects have an important impact on the field dynamics. An exact analytical and numerical solution for the space and time dependencies of an electromagnetic field produced in heavy-ion collisions was presented in Ref. [7]. It was confirmed that nuclear matter plays a crucial role [8] in its time evolution.

In non-central collisions, opposite charge quarks would tend to be emitted in opposite directions relative to the system angular momentum [9–12]. This asymmetry in the emission of quarks would be reflected in an analogous asymmetry between positive- and negative-pion emission directions. This phenomenon is introduced by the large (electro-) magnetic field produced in non-central heavy-ion collisions. The same phenomenon can also be depicted in terms of induction of electric field

by the (quasi) static magnetic field, which happens in the occurrence of these topologically nontrivial vacuum solutions. The induced electric field is parallel to the magnetic field and leads to charge separation in that direction. Thus, the charge separation can be viewed as a nonzero electric dipole moment of the system.

Experimentally, RHIC [13–17] and LHC [18] have published measurements of chiral magnetic effect (CME) by particle correlations, which are qualitatively consistent with the CME. A clear signal compatible with a charge-dependent separation relative to the reaction plane is observed, which shows little or no collision energy dependence when compared to measurements at RHIC energies. It is beneficial to study the nature of the charge-dependent azimuthally correlations observed in RHIC and LHC energy regions [18].

In recent years, much attention [19–23] has been paid to the CME. It has been shown that this effect originates from the existence of nontrivial topological configurations of gauge fields and their interplay with the chiral anomaly, which results in an asymmetry between left- and right-handed quarks. The created strong magnetic field coupled to a chiral asymmetry can induce an electric charge current along the direction of the magnetic

---

Received 23 March 2015

\* Supported by National Natural Science Foundation of China (11375069, 11435054, 11075061, 11221504) and Key Laboratory foundation of Quark and Lepton Physics (Hua-Zhong Normal University) (QLPL2014P01)

1) E-mail: yzhong913@163.com

©2015 Chinese Physical Society and the Institute of High Energy Physics of the Chinese Academy of Sciences and the Institute of Modern Physics of the Chinese Academy of Sciences and IOP Publishing Ltd

field. The strong magnetic field will separate particles of opposite charges with respect to the reaction plane. Recently, possible CME and topological charge fluctuations have been recognized by QCD lattice calculations in gauge theory [24, 25] and in QCD+QED with dynamical 2+1 quark flavors [26]. Thus, such topological and CME effects in QCD might be recognized in relativistic heavy-ion collisions directly in the presence of very intense external electromagnetic fields.

In Refs. [27, 28], we used the Woods–Saxon nucleon distribution instead of a uniform distribution to calculate the magnetic field of the central point for non-central collisions in the RHIC and LHC energy regions in the region of proper time  $\tau \geq 0.02$  fm/c, coming to the conclusion that the magnitude of the magnetic field in the RHIC energy region is larger than that of the magnetic field in the LHC energy region. In this paper, we recalculate the magnetic field using the same model at a much smaller proper time  $\tau \geq 0.0001$  fm/c region, and we find that the magnitude of magnetic field of LHC energy region is larger than that of RHIC energy region at small proper time. We extend the model to calculate the spatial distribution features of the chiral magnetic field of  $-10.0 \text{ fm} \leq x \leq 10.0 \text{ fm}$  and  $-10.0 \text{ fm} \leq y \leq 10.0 \text{ fm}$  in the RHIC and LHC energy regions.

This paper is organized as follows. The key points of the improved model of magnetic field are described in Section 2. The calculation results of the magnetic field are presented in Section 3. A summary is given in Section 4.

## 2 Improved model of chiral magnetic field

The improved model of magnetic field we consider [27, 28] consists of three parts.

(1) As shown in Fig. 1, two similar relativistic heavy nuclei with charge  $Z$  and radius  $R$  are traveling in the positive and negative  $z$  direction with rapidity  $Y_0$ . At  $t=0$  they go through a non-central collision with impact parameter  $b$  at the origin point. The center of the two nuclei are taken at  $x=\pm b/2$  at time  $t=0$  so that the direction of  $b$  lies along the  $x$  axis. The region in which the two nuclei overlap contains the participants, the regions in which they do not overlap contain the spectators.

As the nuclei are nearly traveling with the speed of light in ultra-relativistic heavy-ion collision experiments, the Lorentz contraction factor  $\gamma$  is so large that the two included nuclei can be taken as pancake shape (as the  $z=0$  plane). In Refs. [27, 28], we have used the Woods–Saxon nuclear distribution instead of a uniform nuclear distribution [1].

(2) Secondly, in order to study the strength of the magnetic field caused by the two relativistic traveling

nuclei, we can split the contribution of particles to the magnetic field at the proper time  $\tau > 0$ . The specific forms of expression for the contribution of particles to the magnetic field in the following way

$$\mathbf{B} = \mathbf{B}_s^+ + \mathbf{B}_s^- + \mathbf{B}_p^+ + \mathbf{B}_p^- \quad (1)$$

where  $\mathbf{B}_s^\pm$  and  $\mathbf{B}_p^\pm$  are the contributions of the spectators and the participants moving in the positive or negative  $z$  direction, respectively.

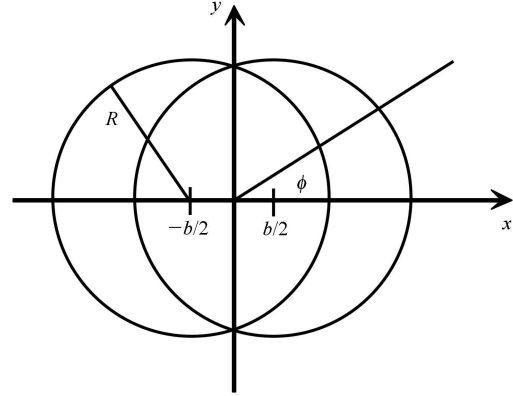


Fig. 1. Cross-sectional view of a non-central relativistic heavy-ion collision along the  $z$  axis. The two nuclei have the same radii  $R$ , move in opposite directions, and collide with impact parameter  $b$ . The angle  $\phi$  is an azimuthal angle with respect to the reaction plane. The plane  $y=0$  is called the reaction plane. The overlap region of the two nuclei contains the participants, and the non-overlap regions contain the spectators.

(3) In order to study the spatial distribution of the magnetic field, we will calculate the  $eB_x$  and  $eB_y$  components of the chiral magnetic field from spectator and participant nuclei. The specific forms of the contribution of  $eB_x$  and  $eB_y$  components from the spectator and participant nuclei are given as follows:

$$\begin{aligned} & eB_{sy}^\pm(\tau, \eta, \mathbf{x}_\perp) \\ &= \mp Z \alpha_{\text{EM}} \sinh(Y_0 \mp \eta) \int d^2 \mathbf{x}'_\perp \rho_\pm(\mathbf{x}'_\perp) \\ & \quad \times [1 - \theta_\mp(\mathbf{x}'_\perp)] \frac{(x' - x)}{[(\mathbf{x}'_\perp - \mathbf{x}_\perp)^2 + \tau^2 \sinh^2(Y_0 \mp \eta)]^{3/2}}, \quad (2) \end{aligned}$$

where  $eB_{sy}$  is the  $y$  component of magnetic field from spectators, and the  $x$  component of magnetic field from spectators is given by:

$$\begin{aligned} & eB_{sx}^\pm(\tau, \eta, \mathbf{x}_\perp) \\ &= \pm Z \alpha_{\text{EM}} \sinh(Y_0 \mp \eta) \int d^2 \mathbf{x}'_\perp \rho_\pm(\mathbf{x}'_\perp) \\ & \quad \times [1 - \theta_\mp(\mathbf{x}'_\perp)] \frac{(y' - y)}{[(\mathbf{x}'_\perp - \mathbf{x}_\perp)^2 + \tau^2 \sinh^2(Y_0 \mp \eta)]^{3/2}}. \quad (3) \end{aligned}$$

The  $y$  component of magnetic field from the participants is given by:

$$eB_{py}^{\pm}(\tau, \eta, \mathbf{x}_{\perp}) = \mp Z\alpha_{EM} \int d^2\mathbf{x}'_{\perp} \int dY f(Y) \sinh(Y \mp \eta) \times \rho_{\pm}(\mathbf{x}'_{\perp}) \theta_{\mp}(\mathbf{x}'_{\perp}) \frac{(x' - x)}{[(\mathbf{x}'_{\perp} - \mathbf{x}_{\perp})^2 + \tau^2 \sinh^2(Y \mp \eta)]^{\frac{3}{2}}}, \quad (4)$$

and the  $x$  component of magnetic field from the participants is given by:

$$eB_{px}^{\pm}(\tau, \eta, \mathbf{x}_{\perp}) = \pm Z\alpha_{EM} \int d^2\mathbf{x}'_{\perp} \int dY f(Y) \sinh(Y \mp \eta) \times \rho_{\pm}(\mathbf{x}'_{\perp}) \theta_{\mp}(\mathbf{x}'_{\perp}) \frac{(y' - y)}{[(\mathbf{x}'_{\perp} - \mathbf{x}_{\perp})^2 + \tau^2 \sinh^2(Y \mp \eta)]^{\frac{3}{2}}}, \quad (5)$$

where  $\tau = (t^2 - z^2)^{1/2}$  is the proper time,  $\eta = \frac{1}{2} \ln[(t+z)/(t-z)]$  is the space-time rapidity, and

$$\theta_{\mp}(\mathbf{x}'_{\perp}) = \theta[R^2 - (\mathbf{x}'_{\perp} \pm \mathbf{b}/2)^2], \quad (6)$$

and the distribution of participants that remain traveling along the beam axis is given by

$$f(Y) = \frac{a}{2 \sinh(aY_0)} e^{aY}, \quad -Y_0 \leq Y \leq Y_0. \quad (7)$$

### 3 Calculation results

#### 3.1 Magnetic field at the central point

As mentioned before, in Ref. [28], we came to the conclusion that the magnitude of magnetic field at the central point in the RHIC energy region is larger than that of the magnetic field in the LHC energy region in  $\tau \geq 0.02$  fm/c region. In this paper, we use a much smaller proper time  $\tau \geq 0.0001$  fm/c to investigate the magnetic field of the central point for non-central collisions in the RHIC and LHC energy regions. Fig. 2 shows the dependencies of magnetic field  $eB$  (at central point  $(x, y) = (0, 0)$ ) on central of mass energy  $\sqrt{s_{NN}}$  at different proper time  $\tau = 0.0001, 0.001, 0.01, 0.1, 1.0, 2.0, 3.0$  fm/c, respectively. It is found that at much smaller proper time ( $\tau = 0.0001$  and  $0.001$  fm/c) the magnetic fields increase with the increase of the CMS energy ( $\sqrt{s_{NN}}$ ). It is argued that the magnitude of magnetic field of LHC energy region is larger than that of RHIC energy region at smaller proper time. But at larger proper time ( $\tau$  larger than  $8.0 \times 10^{-3}$  fm/c), the magnetic field decreases with the increase of collision energy, and the magnitude of magnetic field of the RHIC energy region is larger than that of the LHC energy region. One can find that when  $\tau = 3$  fm/c and  $\sqrt{s_{NN}} > 200$  GeV, the magnetic field approaches zero.

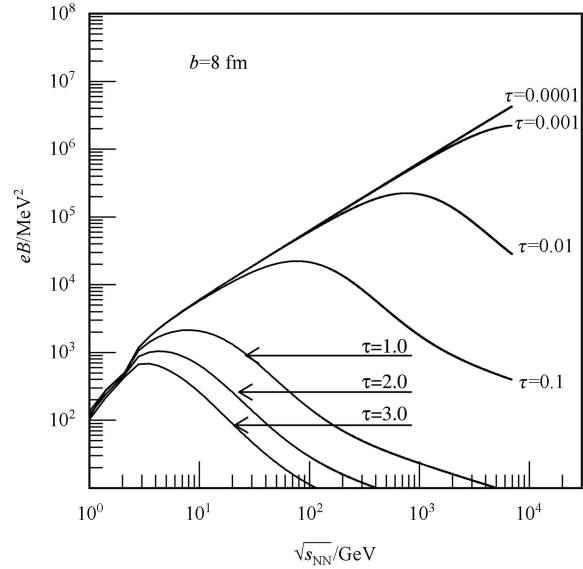


Fig. 2. The dependencies of magnetic field  $eB$  (at central point  $(x, y) = (0, 0)$ ) on centre-of-mass energy  $\sqrt{s_{NN}}$  at different proper time  $\tau = 0.0001, 0.001, 0.01, 0.1, 1.0, 2.0$  and  $3.0$  fm/c, respectively.

In our previous work [27, 28], we did not make a study of the magnetic field contributions from spectator and participant nucleons. An analysis of the magnetic field contributions from spectator and participant nucleons is shown in Fig. 3 in this paper. From Fig. 3(a, b), one can find that at small proper time the magnetic field is mainly from the contribution of spectator nucleons, but as the proper time increases, a larger and larger contribution of the magnetic field is from the participant nucleons. Fig. 3(c, d) show the comparisons of the magnetic field and the ratio of  $(eB)_p/(eB)$  at  $\sqrt{s_{NN}} = 200$  GeV and  $\sqrt{s_{NN}} = 2760$  GeV. One can find that at smaller proper time ( $\tau < 8 \times 10^{-3}$  fm/c) the magnetic field at  $\sqrt{s_{NN}} = 2760$  GeV is greater than that of  $\sqrt{s_{NN}} = 200$  GeV, but when  $\tau > 8 \times 10^{-3}$  fm/c, the magnetic field at  $\sqrt{s_{NN}} = 2760$  GeV is less than that of  $\sqrt{s_{NN}} = 200$  GeV. From Fig. 3(d) one can find that the contribution of magnetic field from participant nucleons increases with the increase of proper time.

#### 3.2 Spatial distributions of magnetic field

For consistency with the experimental results, we take Au–Au collisions with RHIC energy region and Pb–Pb collisions with LHC energy region. When studying the spatial distribution characteristics of magnetic field, we choose the spatial regions of  $-10.0 \text{ fm} \leq x \leq 10.0 \text{ fm}$  and  $-10.0 \text{ fm} \leq y \leq 10.0 \text{ fm}$ .

Figure 4 shows the magnetic field spatial distributions of  $eB_y$  with proper time  $\tau = 0.0001$  fm/c for differ-

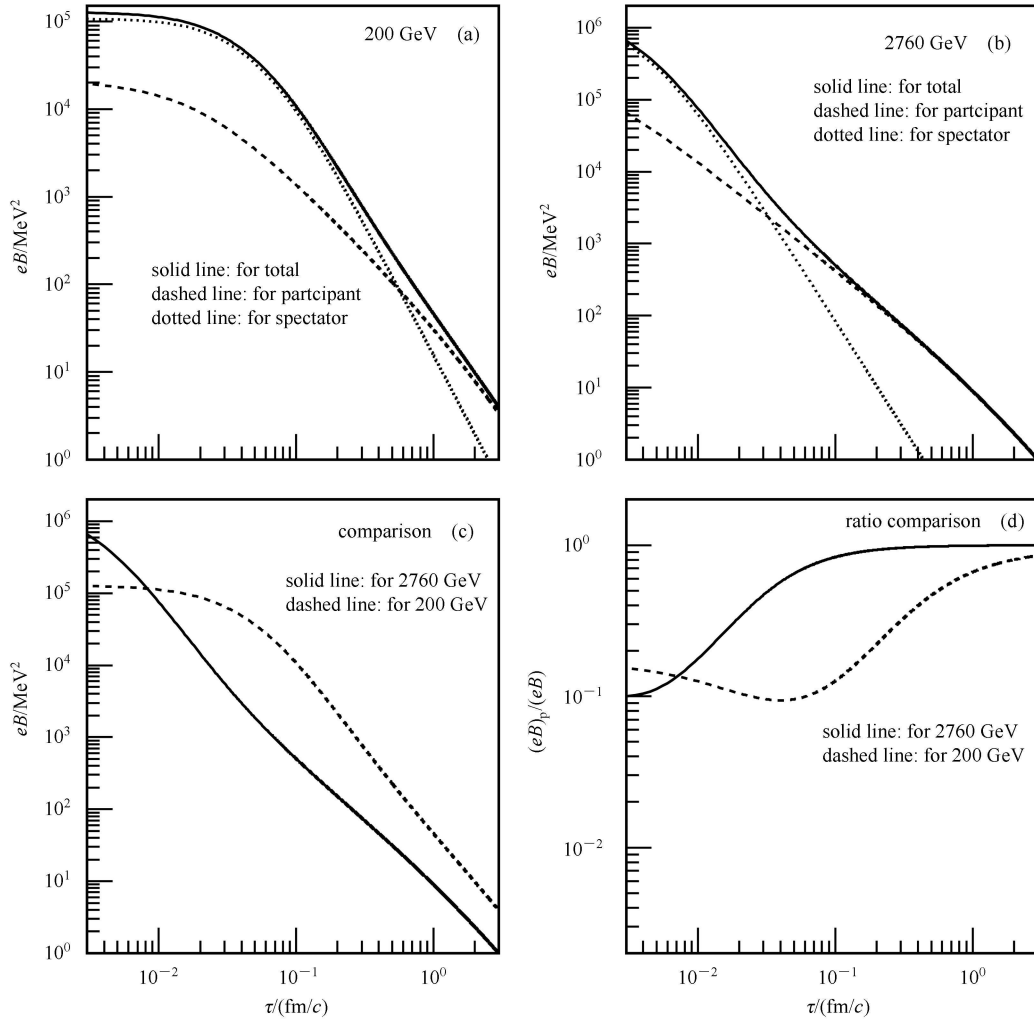


Fig. 3. The dependencies of magnetic field  $eB$  (at central point  $(x, y)=(0, 0)$ ) on proper time  $\tau$  at  $\sqrt{s_{NN}}=200$  GeV (a) for Au–Au collisions with  $b=8$  fm and  $\sqrt{s_{NN}}=2760$  GeV (b) for Pb–Pb collisions with  $b=8$  fm, respectively. The dashed line is for the contribution from participant nucleons, and the dotted line is for the spectator nucleons. The solid line is the combined contributions of participant and spectator nucleons. (c) comparison of the magnetic field between the two collision energies with proper time. (d) comparison of ratio between the magnetic field from participants and the total magnetic field.

ent collision energies  $\sqrt{s_{NN}}=62.4$  GeV, 130 GeV and 200 GeV, respectively. The collision energies shown in Fig. 4 are in RHIC energy region. The spatial distributions of  $eB_y$  show obvious axis symmetry characteristics along the  $x=0$  and  $y=0$  axes. There is a peak region around central point  $(x, y)=(0, 0)$ , and the magnetic field gets smaller and smaller further away from the central position.

The maximum of magnetic field of  $eB_y$  reaches  $8.5 \times 10^4$  when  $\sqrt{s_{NN}}=62.4$  GeV. The maximum increases as the collision energy increases. The maximum of magnetic field  $eB_y$  in RHIC energy region reaches  $2.2 \times 10^5$  MeV<sup>2</sup>.

Compared with Fig. 4, Fig. 5 shows the magnetic field spatial distributions of  $eB_y$  in the LHC energy region. When the collision energy rises to 900 GeV in LHC

energy region, the distribution features of magnetic field have some differences from those of the RHIC energy region. For example the magnetic field distribution peak around  $x=0$  and  $y=0$  becomes flat at  $\sqrt{s_{NN}}=900$  GeV, and the phenomenon of two peaks begins to appear. The maximum of magnetic field  $eB_y$  in LHC energy region reaches  $2.0 \times 10^6$  MeV<sup>2</sup>, which is larger than that of the RHIC energy region at  $\tau=0.0001$  fm/c.

From Fig. 2 to Fig. 5, we argue that the magnetic field spatial distributions of  $eB_y$  are highly inhomogeneous. The distribution features in the RHIC energy region are different from those of the LHC energy region. It is argued that at smaller proper time ( $\tau=0.001$  and  $0.0001$  fm/c) the magnetic fields increase with the increase of CMS energy ( $\sqrt{s_{NN}}$ ), but with the increase

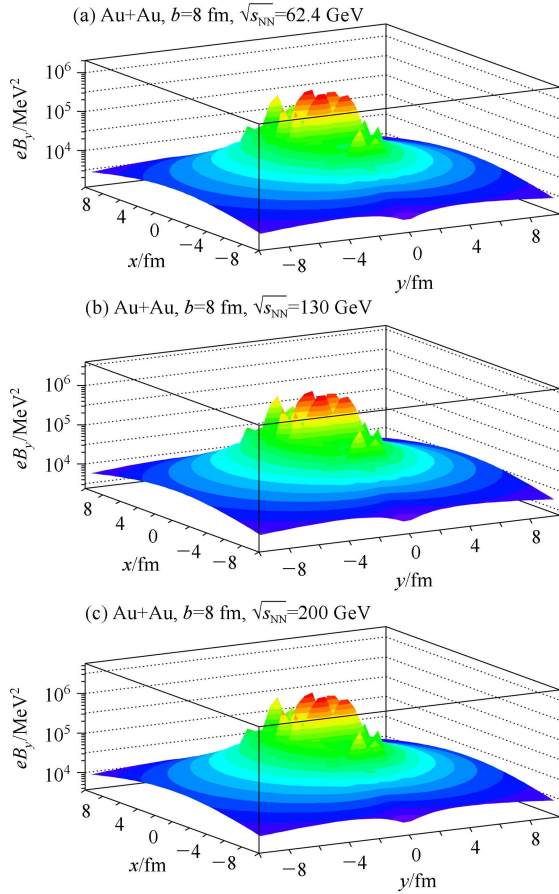


Fig. 4. (color online) The dependencies of magnetic field spatial distributions of  $eB_y$  on different collision energies  $\sqrt{s_{NN}}=62.4$  GeV (a), 130 GeV (b) and 200 GeV (c), respectively. The impact parameters  $b = 8$  fm and proper times  $\tau=0.0001$  fm/c.

of proper time ( $\tau$ ), the magnetic field decreases sharply with increasing collision energy of central of mass  $\sqrt{s_{NN}}$ .

From the above discussion of magnetic field spatial distributions with collision energy and impact parameter relations, we make a study of magnetic field with the proper time. The magnitude of magnetic field is presented as:

$$eB = \sqrt{(eB_x)^2 + (eB_y)^2}. \quad (8)$$

Figure 6 shows the dependencies of the ratio of  $eB_y/(eB)$  on  $x$  and  $y$  at  $\sqrt{s_{NN}}=200$  GeV and at different proper times  $\tau=0.02$ , 0.2 and 2.0 fm/c, respectively. The Fig. 6(a, c and e) show the variation of the ratio of  $eB_y/(eB)$  with  $y$  at different proper times. From Fig. 6(a, c and e), it can be seen that the variation of the ratio of  $eB_y/(eB)$  with  $y$  changes between 0.9 and 1.0. In this case, one can approximate  $eB_y$  instead of  $eB$ . Compared with the relation of ratio  $eB_y/(eB)$  with  $y$ , the dependence of ratio  $eB_y/(eB)$  on  $x$  shown in Fig. 6(b, d

and f) is obviously different. The main difference is the dip located at  $x=0$ . The minimum value of the ratio at  $x=0$  can be decreased to 0.5. This is the reason that one often takes the  $y$  component  $eB_y$  to approximately replace  $eB$ .

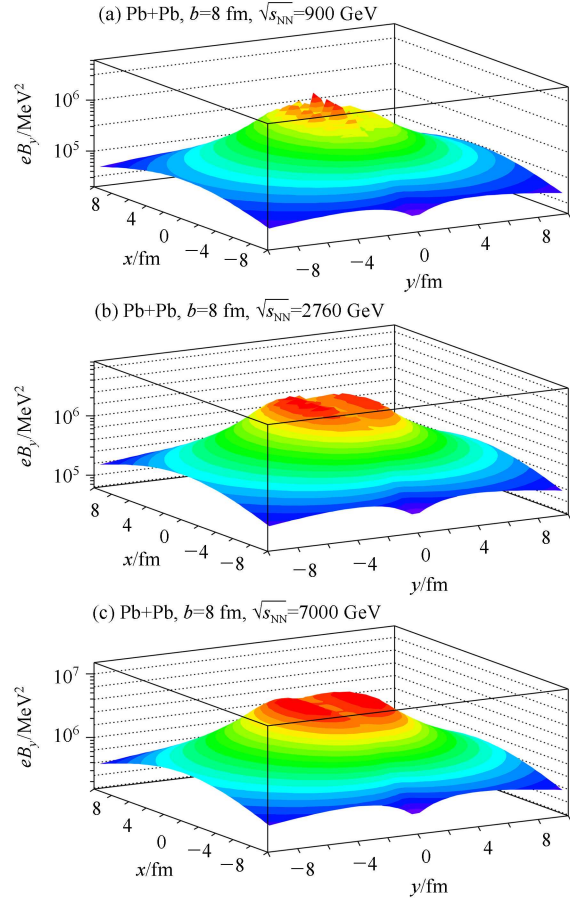


Fig. 5. (color online) The dependencies of magnetic field spatial distributions of  $eB_y$  on different collision energies  $\sqrt{s_{NN}}=900$  GeV (a), 2760 GeV (b), 7000 GeV (c), respectively, with impact parameter  $b=8$  fm and proper time  $\tau=0.0001$  fm/c.

In order to study the spatial distribution of magnetic field with proper time, we show the dependencies of magnetic field  $eB_y$  and  $eB_x$  (at points  $(x, y)=(5, 5)$  and  $(x, y)=(10, 10)$ ) on proper time  $\tau$  at  $\sqrt{s_{NN}}=200$  GeV for Au–Au collisions with  $b=8$  fm and  $\sqrt{s}=2760$  GeV and 7000 GeV for Pb–Pb collisions with  $b=8$  fm, respectively. From Fig.7, one can find that at small proper time the magnetic field increases with the increase of the collision energy, but the magnetic field of  $\sqrt{s}=7000$  GeV decreases more quickly than that of  $\sqrt{s}=200$  GeV with the increase of proper time. Fig. 7(c, d) show that there is a relatively flatter region with proper time at point  $(x, y)=(10, 10)$  than that at point  $(x, y)=(5, 5)$ .

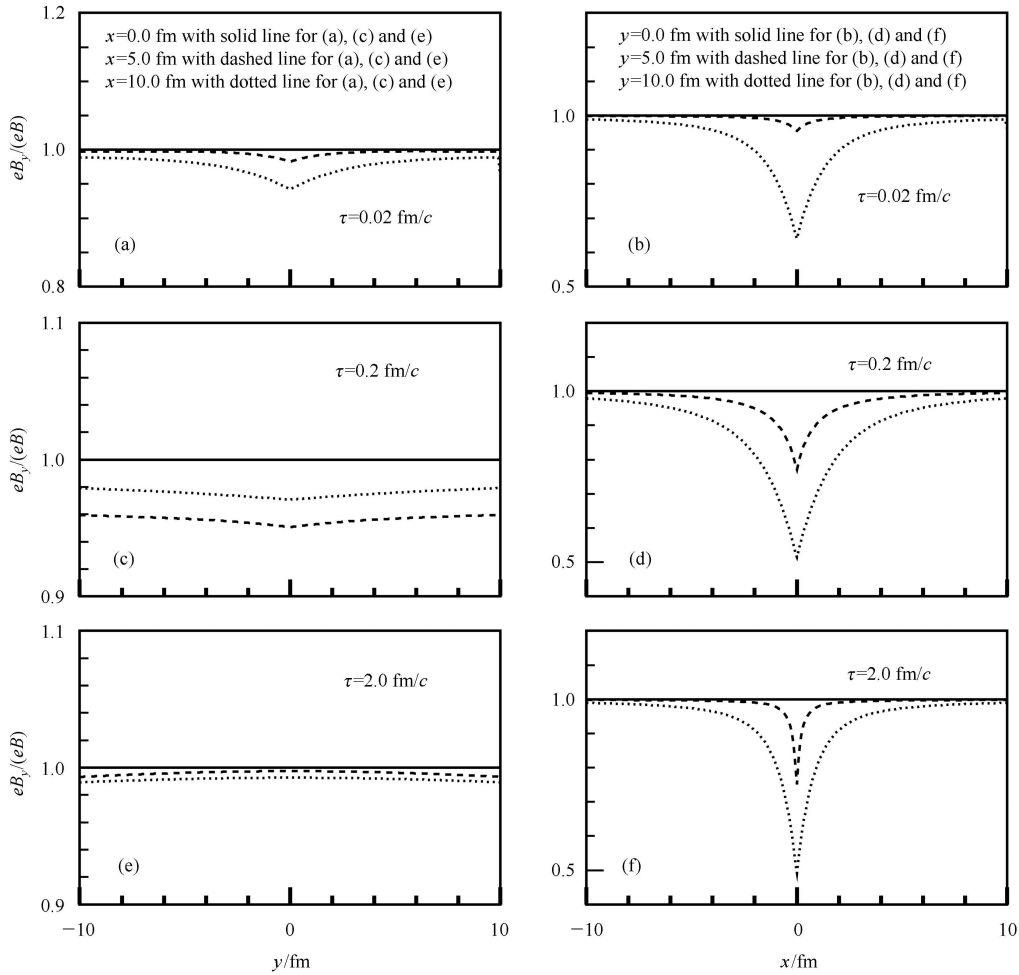


Fig. 6. The dependencies of the ratio of  $eB_y/(eB)$  on  $x$  and  $y$  at  $\sqrt{s_{NN}}=200$  GeV and at different proper times  $\tau=0.02, 0.2$  and  $2.0$  fm/c, respectively. (a), (c) and (e) show the variation of  $eB_y/(eB)$  with  $y$  and (b), (d) and (f) the variation of  $eB_y/(eB)$  with  $x$  at different proper times.

## 4 Summary and conclusion

It is shown that an enormous magnetic field can indeed be created in off-central heavy-ion collisions. The magnetic field distributions of  $eB_y$  are highly inhomogeneous. The enormous magnetic field is produced just after the collision, and the magnitude of magnetic field of LHC energy region is larger than that of RHIC energy region at small proper time ( $\tau < 8.0 \times 10^{-3}$  fm/c). It is found that the magnetic field in the LHC energy region decreases more quickly with the increase of the proper time than that of RHIC energy region. As the proper time  $\tau$  increases to a certain value  $8.0 \times 10^{-3}$  fm/c, the magnitude of magnetic field in the RHIC energy region begins to be larger than that of LHC energy region. These highly inhomogeneous distribution features of RHIC and LHC energy regions given by this paper

will help us to study the experimental results given by RHIC and LHC.

The dependencies of the ratio of  $eB_y/(eB)$  on  $x$  and  $y$  at different collision energies at RHIC and LHC and at different proper time are analyzed in this paper. In most cases, the ratio  $eB_y/(eB)$  approaches 1, so using  $eB_y$  to replace  $eB$  is a good approximation. One should note, however, that the ratio  $eB_y/(eB)$  is between 0.5–1.0 along the  $x=0$  line.

In this paper, we have systematically studied the spatial distribution features of chiral magnetic field in relativistic heavy-ion collisions at the energies reached at LHC and RHIC with the improved model of chiral magnetic field. The features of spatial distributions of chiral magnetic fields at  $\sqrt{s_{NN}}=900, 2760$  and  $7000$  GeV in the LHC energy region and  $\sqrt{s_{NN}}=62.4, 130$  and  $200$  GeV in the RHIC energy region have been systematically studied.

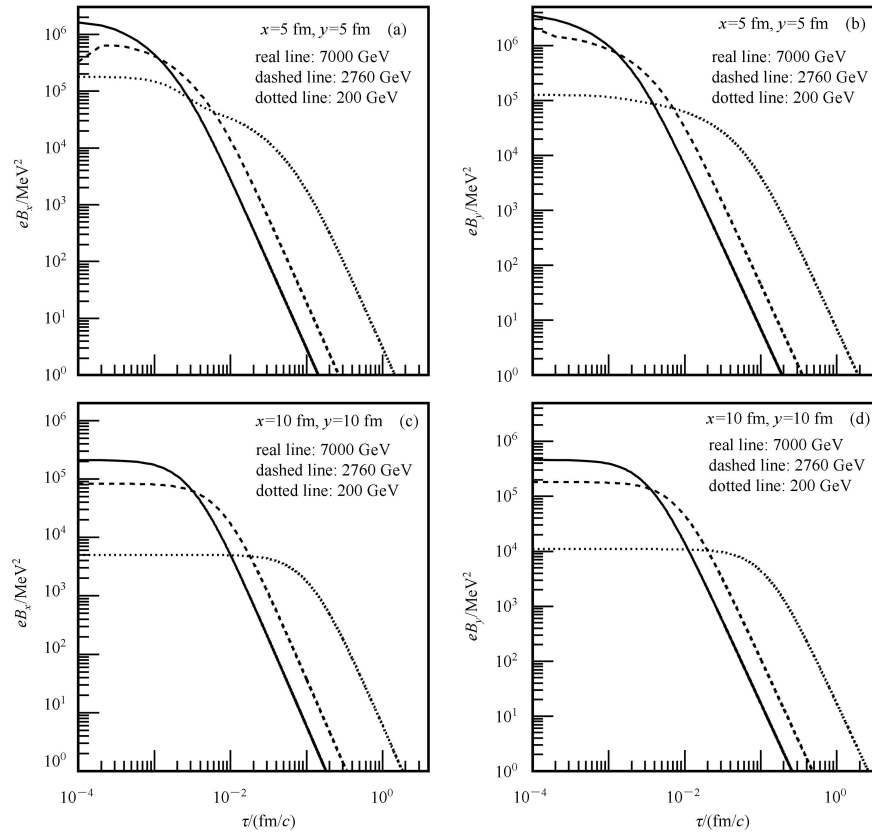


Fig. 7. The dependencies of the magnetic field ( $eB_x$  and  $eB_y$ ) on proper times  $\tau$  at  $(x, y) = (5, 5)$  and  $(10, 10)$  at  $\sqrt{s_{NN}} = 7000, 2760$  and  $200$  GeV respectively. The solid line is  $\sqrt{s_{NN}} = 7000$  GeV, the dashed line is for  $\sqrt{s_{NN}} = 2760$  GeV and the dotted line is for  $\sqrt{s_{NN}} = 200$  GeV.

We have also studied the dependencies of the magnetic field on proper time for RHIC and LHC energy regions, respectively. The maximum position is located at the small proper time ( $\tau \sim 0.0001$  fm/c), more off-central

collisions and  $\sqrt{s_{NN}} \sim 7000$  GeV. The maximum magnetic field in our calculation is about  $eB \simeq 2 \times 10^7$  MeV<sup>2</sup> when  $\tau = 0.0001$  fm/c  $b \simeq 8$  fm and  $\sqrt{s_{NN}} \sim 7000$  GeV.

## References

- 1 Kharzeev D E, McLerran L D, Warringa H J. Nucl. Phys. A, 2008, **803**: 227. arXiv:0711.0950 [hep-ph]
- 2 DENG W T, HUANG X G. Phys. Rev. C, 2012, **85**: 044907
- 3 Bzdak A, Skokov V. Phys. Lett. B, 2012, **710**: 171
- 4 Tuchin K. Advances in High Energy Physics, 2013, **2013**: 490495
- 5 Zakharov B G. Phys. Lett. B, 2014, **737**: 262
- 6 Gürsoy U, Kharzeev D E, K Rajagopal K. Phys. Rev. C, 2014, **89**: 054905
- 7 Tuchin K. Phys. Rev. C, 2013, **88**: 024911
- 8 Tuchin K. Phys. Rev. C, 2010, **82**: 034904; Tuchin K. Phys. Rev. C, 2011, **83**: 039903
- 9 Kharzeev D E, Zhitnitsky A. Nucl. Phys. A, 2007, **797**: 67
- 10 Kharzeev D E. Phys. Lett. B, 2006, **633**: 260
- 11 Voloshin S A, ZHANG Y. Z. Phys. C, 1996, **70**: 665
- 12 Voloshin S A. Phys. Rev. C, 2004, **70**: 057901
- 13 Abelev B I, Aggarwal M M, Ahammed Z et al. Phys. Rev. Lett. 2009, **103**: 251601
- 14 Abelev B I, Aggarwal M M, Ahammed Z et al. Phys. Rev. C, 2010, **81**: 054908
- 15 Selyuzhenkov I V, STAR Collaboration. Romanian Reports in Physics, 2006, **58**: 49
- 16 Voloshin S A, STAR Collaboration. Nucl. Phys. A, 2009, **830**: 377
- 17 Ajitanand N N, Lacey R A, Taranenko A, Alexander J M et al. Phys. Rev. C, 2011, **83**: 011901
- 18 Abelev B I, Adam J, Adamova D et al. Phys. Rev. Lett., 2013, **110**: 012301
- 19 Kharzeev D E, Pisarski R D, Tytgat M N G. Phys. Rev. Lett., 1998, **81**: 512
- 20 Kharzeev D E, Pisarski R D, Tytgat M N G. Phys. Rev. D, 2000, **61**: 111901
- 21 Kharzeev D E. Phys. Lett. B, 2006, **633**: 260
- 22 Fukushima K, Ruggieri M, Gatto R. Phys. Rev. D, 2010, **81**: 114031
- 23 Kharzeev D E, Warringa H J. Phys. Rev. D, 2009, **80**: 034028
- 24 Buividovich P V, Chernodub M N, Luschevskaya M N, Polikarpov M I. Phys. Rev. D, 2009, **80**: 054503
- 25 Buividovich P V, Chernodub M N, Luschevskaya M N, Polikarpov M I. Phys. Rev. D, 2010, **81**: 036007
- 26 Abramczyk M, Blum T, Petropoulos G, ZHOU R. PoS (LAT2009), 2009, 181
- 27 MO Y J, FENG S Q, SHI Y F. Phys. Rev. C, 2013, **88**: 024901
- 28 ZHONG Y, YANG C B, CAI X, FENG S Q. Advances in High Energy Physics, 2014, **2014**: 193039